IEEE Access
Multidisciplinary | Rapid Review | Open Access Journal

Received August 12, 2019, accepted August 26, 2019, date of publication September 9, 2019, date of current version September 23, 2019.

Digital Object Identifier 10.1109/ACCESS.2019.2939806

Analysis and Design of a Broadband Metasurface-Based Vortex Beam Generator

WEN-LONG GUO, GUANG-MING WANG, (Member, IEEE), HAI-PENG LI, HAI-SHENG HOU, AND HE-XIU XU, (Senior Member, IEEE)
Air and Missile Defend College, Air Force Engineering University, Xi'an 710051, China

Corresponding authors: Guang-Ming Wang (wgming01@sina.com) and He-Xiu Xu (hxxuellen@gmail.com)

This work was supported in part by the National Natural Science Foundation of China under Grant 61871394, and in part by the Key Program of National Natural Science Foundation of Shaanxi Province under Grant 2017KJXX-24.

ABSTRACT Metasurface-based vortex beam generators are very promising and applicable to enhance transmission data capacity in wireless communication system. However, most designs to date are ceased to predict their far-field characteristic, which is actually in demand when applied to wireless communication. Here, we find for the first time a deterministic and robust strategy to fastly estimate the exact far-field patterns and gain limit of a vortex beam based on the theoretical analysis of aperture field with spiral phase profile. For verification, a broadband metasurface-based vortex-beam generator based on geometric phase is designed, numerically calculated and experimentally measured at microwave regime. Excellent agreements are observed among far-field results obtained based on the proposed method, numerical simulations and experimental measurements, firmly demonstrating the validity and correctness of the proposed strategy. Such a deterministic and robust strategy of predicting far-field characteristics of a vortex beam may pave the way for its applications in many engineering scenarios, such as conical beam design, wireless communication, et al.

INDEX TERMS Metasurface, orbital angular momentum, conical beam.

I. INTRODUCTION

According to optical theory, momentums of electromagnetic (EM) wave primarily correspond to spin angular momentum (SAM) and orbital angular momentum (OAM) [1]–[10]. Mainly associated with the polarized status of a beam, SAM only holds two possible modes that are orthogonal to each other [2]. But for OAM, it has unlimited topological charges since different charges are mutually orthogonal to each other, which finally results in the OAM's capability of increasing communication channels [3]–[8]. Based on this, massive efforts are devoted to generating vortex beams carrying OAM in microwave region [9]–[15].

To date, various methods, such as employing circular-phased arrays [16], spiral phase plate [17] and metasurfaces [18]–[21], et al, have been reported to exhibit spiral phase distribution to generate OAM beams with single or multiple modes. It is particularly true for a circular-ring phased array to generate vortex beam carrying OAM and unambiguously estimate its far-field characteristic by using vector field-sensing electric and magnetic triaxial antennas [22]. But it can not be neglected that complicated architecture and high cost of the phased arrays highly restrict their applications [22], [23]. For a spiral phase plate, it is mostly realized by the accumulation of phase delays during wave propagation, which suffers from large profile and significant thickness especially in microwave region. Nevertheless, the recently developed metasurfaces that are able to flexibly tailor wavefront by introducing abrupt phase change have been proved to be an effective method to generate a vortex beam carrying OAM with low profile, low loss, low cost and easy fabrication [24]–[29]. And to date, numerous meta-devices implemented by metasurfaces have been demonstrated in microwave region to generate broadband OAM, [30] high-efficiency OAM, [31] multi-mode OAM [32] and even circularly decoupled OAM, [33] et al. But almost all the reported metasurface-based OAM generators are ceased to predict their far-field performances. Besides, it should be noted that the reported prediction method of a circularly phased array to generate OAM is not suitable for a metasurface-based vortex beam generator because performances of metasurfaces all rely on the periodic or quasi-periodic boundary condition that is a

The associate editor coordinating the review of this manuscript and approving it for publication was Muhammad Zubair.

difficult requirement for a circularly phased array to meet [22], [29]. That is, the huge potential for OAM to enhance data capacity in wireless communication and the powerful capability of metasurface to generate OAM both beckon for a new strategy to theoretically predict far field characteristics of a vortex beam implemented by metasurfaces.

This paper focuses on a novel strategy to predict and assess the far-field characteristic of a metasurface-based vortex beam generator. We consider the spiral phase profile as a discrete sampling of a continuous counterpart, and believe it is true that the far-field characteristics are well agreed when sampling interval of a discrete phase profile satisfies Shannon sampling theory. Then we find that with analysis of the continuous field of an aperture with vortex phase profile, a compact and robust strategy can be established to fast estimate far-field characteristic of a metasurface-based vortex beam generator. Furthermore, the configured strategy is well validated by antenna array theory, FDTD simulations and carefully implemented experiments. The proposed strategy as well as the design and analysis of a metasurface-based vortex beam generator in this paper may pave the way for the application of vortex beam generators to wireless communications.

II. ANALYSIS FOR VORTEX PHASE PLATE

To generate a vortex beam by employing a metasurface, the key is to introduce a spiral phase profile described by $e^{jl\varphi}$, in which l is the topological mode or charge. In this way, the phase distribution imposed on the surface can be described as

$$\Phi\,(x, y) = l\tan^{-1}(\frac{y}{x}). \tag{1}$$

When described in a polar coordinate system, the required phase profile in (1) can be written as

$$\Phi\,(r, \varphi) = l\varphi. \tag{2}$$

With this in mind, we correspondingly show the theoretical background and the proposed strategy for estimating far-field characteristic of a vortex phase plate.

A. THEORETICAL BACKGROUND

For a circular-ring phased array, [22] reported a method to unambiguously estimate the OAM in radio beams with the use of vector field-sensing electric and magnetic tri-axial antennas. As depicted in Fig. 1, the element in the phased array is characterized with a spiral phase of $\Phi = 2l\pi n/N$(discretized form of (2)), in which n depicts the nth element while N shows the element number. Based on the antenna array theory and an assumption that N is sufficiently large, the array factor can be approximately written as [22]

$$\begin{aligned}\Psi_l\,(\theta, \varphi) &= \sum_{n=1}^{N} e^{-j\left(\vec{k}\cdot\vec{r}_n - l\varphi_n\right)} \\ &\approx \frac{Ne^{jl\varphi}}{2\pi}\int_0^{2\pi} e^{-jka\sin\theta\cos\varphi}\end{aligned}$$

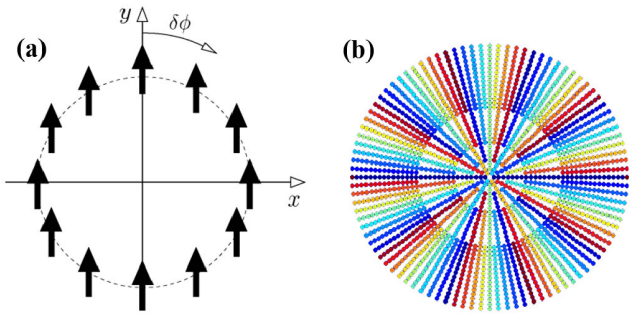

FIGURE 1. (a) Circular-ring phased array in [22] and (b) multi rings distribution of a metasurface-based conical beam generator in [29].

$$= Nj^{-l}e^{jl\varphi}J_l(ka\sin\theta), \tag{3}$$

in which l corresponds to the topology mode whereas a and k represent the ring radius and wave number in free space. It is particularly true for this method to estimate the OAM in radio beams, but it is also true that this method is only appropriate to the configuration of a circular phase ring. To expand a ring to a circular surface, multiple rings are assembled to form a surface like [29] as depicted in Fig. 1(b). Therein, the array factor of $F_l(\theta, \varphi)$ can be calculated by integrating the equation in (3) with different radius as [29]

$$F_l\,(\theta, \varphi) \approx \sum_{m=1}^{M} N_m j^{-l}e^{jl\varphi}J_l(ka_m\sin\theta), \tag{4}$$

in which N_m and a_m correspond to the element number and radius of the mth ring. We emphasize that this method may destroy the quasi-periodic boundaries for meta-atoms when it is applied to metasurface-based vortex beam generator. Moreover, it's still a sophisticated strategy to estimate the vortex beam in radio frequencies and may be more complicated and time consuming when elements in each ring are different from each other.

B. PROPOSED STRATEGY FOR FAST ANALYSIS

To establish a strategy for estimating far-field characteristic of a metasurface-based vortex beam generator, the quasi-periodic boundaries should be always satisfied to ensure each element holding a precise and stable phase response.

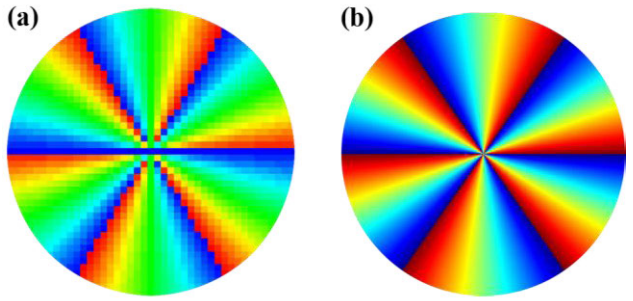

FIGURE 2. (a) Discrete spiral phase profile in steps of a confirmed lattice constant. (b) Continuous spiral phase profile with topological charge of 6.

For this reason, we are prone to adopt the configuration of lattice distribution as unambiguously depicted in Fig. 2(a). As is well known, the resulting far-filed characteristic of the discrete phase distribution in Fig. 2(a) well matches that of the continuous phase profile in Fig. 2(b) under the condition that lattice spacing satisfies Shannon sampling theory. In view of this, we first assume that the phase plate in Fig. 2(b) is with uniform E- and H-field distribution. Then an infinitesimal panel on the surface, which is always defined as a Huygens panel, is equivalent to the superposition of a current element and a magnetic current element, which can be denoted by

$$\boldsymbol{J}_S = \boldsymbol{e}_n \times \boldsymbol{H}, \quad \boldsymbol{J}_{mS} = -\boldsymbol{e}_n \times \boldsymbol{E}, \tag{5}$$

in which $\boldsymbol{e_n}$ denotes the normal vector of the surface. This kind of infinitesimal panel characterized by (5) is well known for its normalized far-field pattern as shown as below

$$F(\theta) = \frac{1+\cos\theta}{2}. \tag{6}$$

By integrating the infinitesimal panels on the surface as depicted in Fig. 3, we can derive out the E-field at the point of P that is located in the far-field region.

$$E_P = j\frac{1}{2\lambda r}(1+\cos\theta)\int_S e^{-jkr'}e^{-jl\varphi'}dS. \tag{7}$$

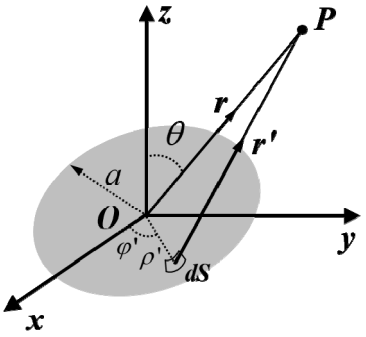

FIGURE 3. Schematic of the relative location relationship between the far field point P and the circular source surface.

Considering that the resulting conical beam is with global rotational symmetric, we only need to calculate the E-field distribution on the plane with azimuth angle of $\varphi = 90°$. Thus the distance between the far-field point P and the infinitesimal panel of dS will be

$$r' = r - \rho'\sin\theta\sin\varphi'. \tag{8}$$

By combining equations (7) and (8), E_P can be written as

$$E_P\big|_{\varphi=90} = j\frac{e^{-jkr}}{2\lambda r}(1+\cos\theta)\int_S e^{j(k\rho'\sin\theta\sin\varphi'-l\varphi')}\rho' d\varphi' d\rho'. \tag{9}$$

Mathematically, such a form of E_P in (9) can be further simplified as

$$E_P\big|_{\varphi=90} = j\frac{\pi a^2 e^{-jkr}}{\lambda r}\cdot\frac{(1+\cos\theta)}{2}\cdot\frac{2\psi_0 J_{l+1}(\psi_0)+2l\int_0^{\psi_0}J_{l+1}(x)dx}{\psi_0^2} \tag{10}$$

in which $\Psi_0 = ka\sin\theta$ and a is denoted by the radius of the circular surface, J represents the Bessel function and k is the wave number in free space. Finally, we configure the directional function of a circular plate with spiral phase profile as demonstrated as below

$$F(\theta,\varphi) = \frac{(1+\cos\theta)}{2}\cdot\frac{2\psi_0 J_{l+1}(\psi_0)+2l\int_0^{\psi_0}J_{l+1}(x)dx}{\psi_0^2}, \quad \Psi_0 = ka\sin\theta, \tag{11}$$

in which $F(\theta,\varphi)$ represents the directional function whereas θ and φ show the elevation and azimuth angle. Herein, the directional function is normalized to the case of $l = 0$ which actually represents a plate in phase and with uniform E-field distribution. That is, the case of $l = 0$ illustrates the gain limit of an aperture. In this way, the compact expression of directional function can not only predict far-field pattern of a vortex beam, but also illustrate its theoretical gain limit compared with a same area in phase with uniform E-field distribution.

III. VALIDATION OF THE PROPOSED STRATEGY

Based on abovementioned analysis, a metasurface-based vortex beam generator will be devised, simulated and then measured to strongly validate the proposed strategy from both EM simulation and physical experiment. Before that, the proposed compact strategy will be first verified by the time-consuming theory of antenna array.

A. VALIDATION BY ANTENNA ARRAY THEORY

We first employ the antenna array theory to validate the proposed strategy. Generally, the directivity of an array can be written as

$$F(\theta,\varphi) = f(\theta,\varphi)\cdot S(\theta,\varphi). \tag{12}$$

in which $f(\theta,\varphi)$ is the directivity of the meta-atom, whereas $S(\theta,\varphi)$ is the array factor. Considering the source as a Huygens panel, we will obtain

$$f(\theta,\varphi) = \frac{1+\cos\theta}{2} \tag{13}$$

$$S(\theta,\varphi) = \sum_{m=0}^{N-1}\sum_{n=0}^{N-1} e^{j\Phi_{mn}}e^{jkd\sin\theta(m\cos\varphi+n\sin\varphi)}, \quad r \le r_0 \tag{14}$$

Herein, r_0 denotes the radius of the circular array while Φ_{mn} represents the phase shift of the element in m-th row and n-th column. Besides, d represents the element interval. In this way, the functional direction of an array with circular boundary can be obtained by combining (12) – (14)

$$F(\theta,\varphi) = \frac{1+\cos\theta}{2}\cdot\left(\sum_{m=0}^{N-1}\sum_{n=0}^{N-1} e^{j\Phi_{mn}}e^{jkd\sin\theta(m\cos\varphi+n\sin\varphi)}\right), \quad r \le r_0. \tag{15}$$

We first contribute our attention to the radiation intensity at the maximum radiation direction and the direction itself versus topology charge of a vortex beam. Due to the resulted conical beam of a vortex phase plate, the maximum radiation direction just corresponds to an elevation angle. With elements number set as 45 and lattice spacing fixed at 5mm, the results at 14GHz calculated by antenna array theory, as shown in Fig. 4, are in excellent agreement with those predicted by (11), both indicating a decline of intensity at the direction of maximum radiation and a gradual increase of radiation angle when topology of a vortex beam ranges from 1 to 10. Since the intensities are all normalized to the case of $l = 0$ which represents the gain limit of an aperture, the results depicted in Fig. 4 also illustrate the gain limit of an aperture with spiral phase profile. In Fig. 5(a) and (b), we show how the maximum radiation angle changes when operating frequency and aperture diameter vary with topology charge l setting as 0, 4 and 6. Clearly, the well matched results not only prove the validity of our proposed strategy for estimating a vortex beam but also show that the radiation angle decreases with both frequency and aperture diameter. This can be interpreted that the larger electrical size will contribute to smaller beam width of an aperture thus to little conical angle of a vortex beam. We finally validate the validity of our proposed strategy by calculating far-field patterns at different frequencies with (11) and (15) respectively. As unanimously depicted in Fig. 6, the coincident curves vividly show that our proposed method is a powerful strategy to predict both far-field pattern and maximum radiation angle. All in all, the proposed strategy is well validated by antenna array theory and will be further proved by FDTD simulations and firmly validated by experiment in what follows.

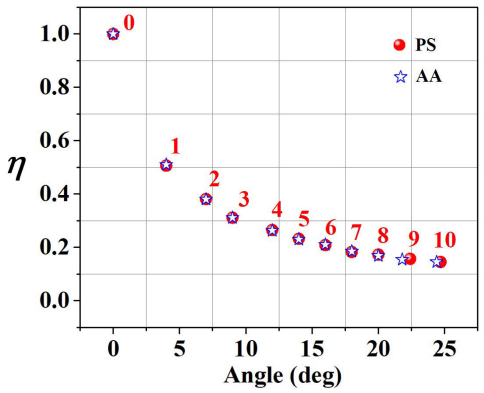

FIGURE 4. The maximum radiation direction (elevation angle) and intensity versus topology mode of the vortex beam carrying OAM. Herein, η depicts the amplitude of E-field at the maximum radiation direction that is normalized to l = 0. PS represents the results from the proposed strategy in this paper, while AA depicts those obtained from antenna array theory.

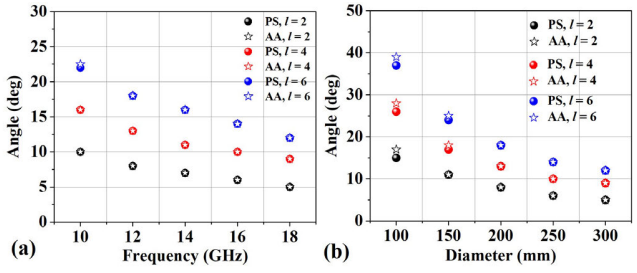

FIGURE 5. Maximum radiation angle (elevation angle) of a vortex beam versus (a) frequency with element spacing set as 5mm and aperture diameter of 225mm and (b) diameter with element spacing set as 5mm and frequency of 14GHz.

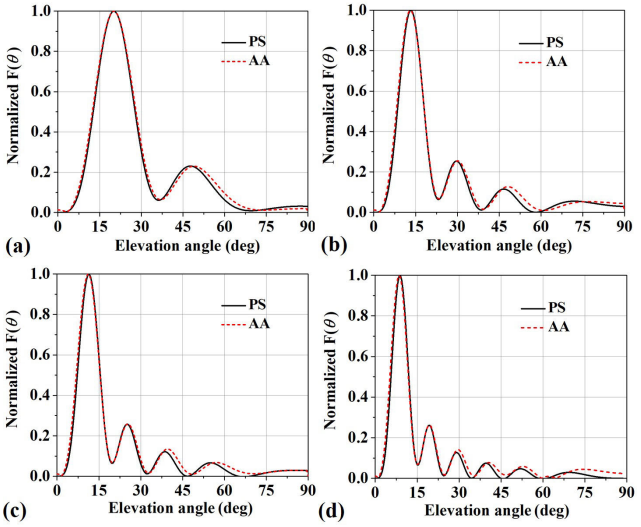

FIGURE 6. Normalized E-field patterns versus elevation angle at (a) 8 GHz (b) 12 GHz (c) 14 GHz and (d) 18 GHz calculated by the proposed strategy (PS) and antenna array (AA) theory with azimuth fixed at 90°.

B. VALIDATION BY SIMULATION

As shown in Fig. 7, a classical quasi-I-shaped meta-atom is first optimized to meet the requirement of geometric phase principle. In particular, the element consists of a quasi-I-shaped metallic pattern and a metallic ground separated by a dielectric substrate of FR4 with relative dielectric constant of 4.3, dissipation factor of 0.003, and a thickness of $h = 2.5$mm. Concrete parameters of the element are denoted by $d = 0.2$mm, $d_1 = 0.4$mm, $p = 5$mm and $\varphi = 104°$. The metallic pattern and ground are both made of copper thin film with thickness of 0.036mm. As is well known, the complex

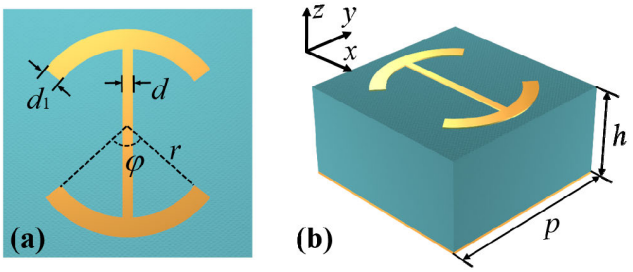

FIGURE 7. (a) Top and (b) perspective view of the optimized meta-atom with geometric phase.

reflection coefficient of an arbitrary reflective meta-atom for right hand circularly polarized (RHCP) wave and left hand circularly polarized (LHCP) wave excitations can be obtained by [30]:

$$r_{rr} = \frac{1}{2}\left[(r_{xx} - r_{yy}) + j(r_{xy} + r_{yx})\right] e^{j2\alpha}. \quad (16)$$

$$r_{ll} = \frac{1}{2}\left[(r_{xx} - r_{yy}) - j(r_{xy} + r_{yx})\right] e^{-j2\alpha}. \quad (17)$$

in which α represents the rotation angle of the element, and r_{xx} and r_{yy} are the co-polarized reflection coefficients under x- and y-polarized normal incidence, whereas r_{yx} and r_{xy} are the cross-polarized reflection coefficients. Since the element depicted in Fig. 7 is symmetrical about x and y axes, none of crosstalk will be excited when the surface is impinged by x- or y-polarized incidence. Thus the primary target of optimizing the element is to achieve a phase difference of 180° between r_{xx} and r_{yy}. In Fig. 8(a), we simulate the meta-atom in CST Microwave Studio with unit cell boundaries set in x and y directions and then calculate and depict the phase difference between r_{xx} and r_{yy}. Clearly, the relative parallel phase curves can always hold a near 180° phase difference across the bandwidth of 8 - 18 GHz. Based on (17) and an assumption of lossless case for the meta-atom, the reflection coefficient of the element under LHCP incidence can be simplified as $r_{ll} = \left|1 - e^{j\Delta\Phi}\right|/2$ with $\Delta\Phi$ indicating the phase difference of Φ_{xx} and Φ_{yy}. In this regard, the reflectivity under circularly polarized incidence can be deduced above 0.9 across the whole band of 8-18 GHz from Fig. 8(a), which has been firmly verified from Fig. 8(b) that illustrates the reflective amplitude and phase of the element with LHCP wave excitation. And as expected, the reflective phase variation is precisely twice the rotation angle, which well matches the predicted angle variation shown in (17).

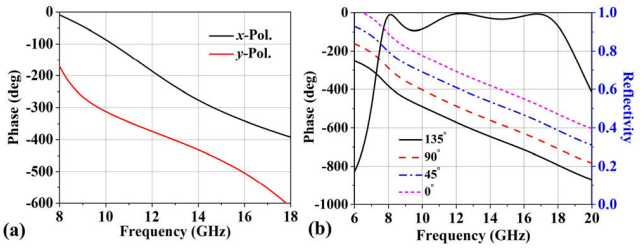

FIGURE 8. (a) Co-polarized phase response of the meta-atom under x- and y-polarized incidence. (b) Reflectivity and phase response of the element changing with different rotation angles under the incidence of LHCP wave.

To implement vortex beams by the proposed element, a LHCP phase profile characterized by $e^{-j4\varphi}$ as depicted in Fig. 9(a) is imposed on the surface. Notably, 360° has been subtracted from any phase exceeding 360° for easy realization. Based on the phase profile and the relationship between phase shift and the rotation angle, a metasurface is first configured to a square array with 45 × 45 elements and then simplified to an array with circular boundary by deleting elements out of the circle with diameter of 225mm,

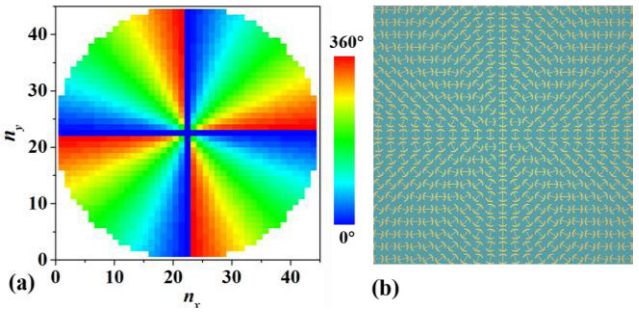

FIGURE 9. (a) Phase profile and (b) layout of the designed metasurface-based vortex beam generator.

which finally results in a circular phase plate of diameter of 225mm. In Fig. 9(b), we only show a part view of the circular phase plate to give a clear view of the structure of the configured metasurface. To illustrate performances of the configured metasurface, we numerically characterize the designed metasurface through FDTD simulations in CST Microwave Studio. Fig. 10 depicts the calculated near-field distribution on the observed plane of $z = 200$mm and the far-field patterns at 8, 12, 14 and 18GHz. Notably, the results referred to Re(E_x) and abs(LHCP) are all normalized to their maximal intensity for convenience and clear identification. Unambiguously, the near field results well illustrate a vortex beam with topology charge of 4 from 8 to 18GHz, which is further validated by the far-field results that exhibit amplitude null at the central region and a full 8π spiral phase range during one revolution.

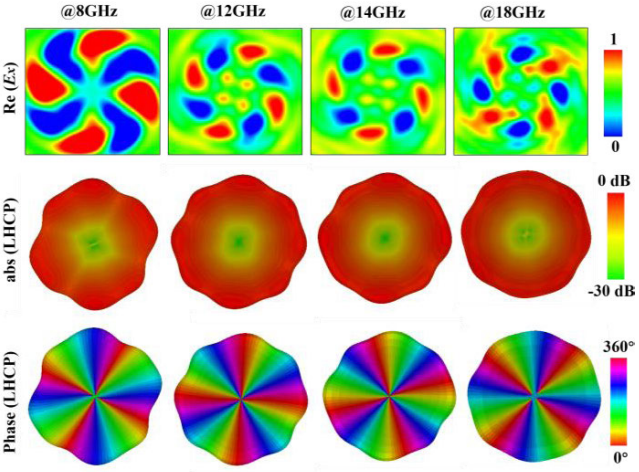

FIGURE 10. Numerically calculated near-field (top row) and far-field (bottom row) patterns of the configured vortex metasurface.

C. VALIDATION BY EXPERIMENT

To further prove the generated conical beam, a metasurface prototype is fabricated by the printed-circuit-board (PCB) technology and then measured in an anechoic chamber to avoid unwanted interference from surroundings. Figs. 11(a) and (b) show the fabricated metasurface sam-

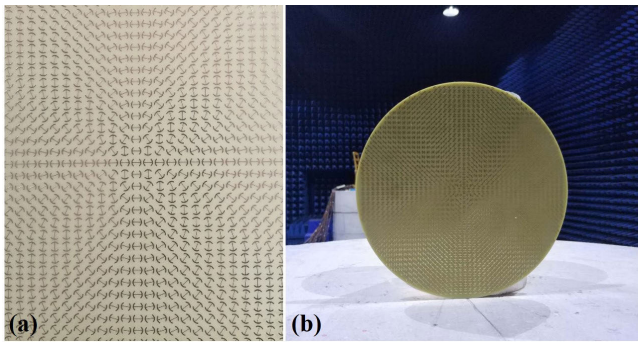

FIGURE 11. (a) Part view of the fabricated prototype and (b) far-field measurement setup of the metasurface-based vortex beam generator.

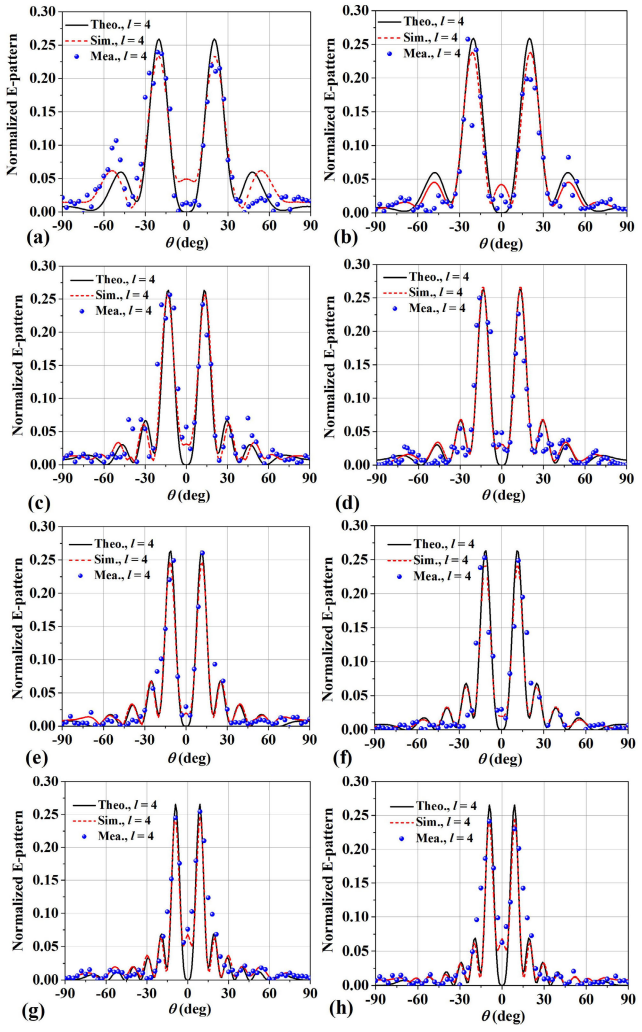

FIGURE 12. Normalized E-field patterns at (a) ∼ (b) 8GHz, (c) ∼ (d) 12GHz, (e) ∼ (f) 14GHz, (g) ∼ (h) 18GHz. Notably, (a), (c), (e) and (g) correspond to the patterns on xoz plane, while (b), (d), (f) and (h) refer to the patterns on yoz plane.

ple and the experimental setup to measure the far-field pattern. In particular, the prototype is placed on a rotated platform (made by foam) to be rotated in azimuth angle and impinged by a beam of quasi plane wave emitted from a horn source. In addition, another horn source is placed in the same horizontal plane with the prototype so as to record the scattering pattern of the metasurface. In Fig. 12 we show the most concerned issues of far-field patterns that are first theoretically calculated by the proposed strategy, then numerically simulated and finally experimentally measured. It should be noted that the results are all E-patterns which are normalized to the theoretical case of $l = 0$. The case of $l = 0$ is implemented by impinging a same-sized metallic plate with a beam of plane wave, which actually shows the gain limit of a plane aperture. To exhibit the pattern stability of the conical beam resulted from the spiral phase profile, the measured results from 8GHz to 18GHz are all depicted in Fig. 12. Despite fluctuation existing in some directions, the measured and simulated far-field results both well match the theoretically calculated ones, which further verify the validity of the proposed strategy for estimating far-field patterns of a vortex plate and firmly prove the operating bandwidth of the generator. Combining the demonstrated results in simulation setup, we further believe that the MS performs well in generating conical beam carrying OAM for circularly-polarized wave over a broad frequency range from 8 GHz to 18 GHz. Besides, far-field performances of such kind of metasurface-based vortex beam generators can be fast and easily predicted by the proposed strategy.

IV. CONCLUSION

In conclusion, a novel strategy is proposed to exactly estimate far-field patterns of vortex beams that are especially carried out by metasurfaces. Verified by antenna array theory, FDTD simulations and experimentally measured results, the proposed strategy can not only predict far-field patterns but also exactly illustrate the maximum radiation direction as well as the gain limit of a metasurface-based vortex beam. Furthermore, the illustrated design of a broadband metasurface-based vortex beam generator well shows powerful capabilities of metasurfaces for wavefront engineering. All in all, the analysis and the design of a metasurface-based vortex beam generator in this paper may promote the application of metasurface to vortex beam generator carrying OAM and further promote application of vortex beams to wireless communication to improve transmission data rate.

REFERENCES

[1] L. Allen, M. W. Beijersbergen, R. J. C. Spreeuw, and J. P. Woerdman, "Orbital angular momentum of light and the transformation of Laguerre–Gaussian laser modes," *Phys. Rev. A, Gen. Phys.*, vol. 45, no. 11, pp. 8185–8189, 1992.

[2] W.-L. Guo, G.-M. Wang, K. Chen, H.-P. Li, Y.-Q. Zhuang, H.-X. Xu, and Y. Feng, "Broadband polarization-conversion metasurface for a Cassegrain antenna with high polarization purity," *Phys. Rev. Appl.*, vol. 12, no. 1, 2019, Art. no. 014009.

[3] M. Padgett, J. Courtial, and L. Allen, "Light's orbital angular momentum," *Phys. Today*, vol. 57, no. 5, p. 35, 2004.

[4] Z. Zhao, J. Wang, S. Li, and A. E. Willner, "Metamaterials-based broadband generation of orbital angular momentum carrying vector beams," *Opt. Lett.*, vol. 38, no. 6, pp. 932–934, 2013.

[5] G. A. Turnbull, D. A. Robertson, G. M. Smith, L. Allen, and M. J. Padgett, "The generation of free-space Laguerre–Gaussian modes at millimetre-wave frequencies by use of a spiral phaseplate," *Opt. Commun.*, vol. 127, pp. 183–188, Jun. 1996.

[6] H. Chen, J. Hao, B.-F. Zhang, J. Xu, J. Ding, and H.-T. Wang, "Generation of vector beam with space-variant distribution of both polarization and phase," *Opt. Lett.*, vol. 36, no. 16, pp. 3179–3181, Aug. 2011.
[7] M. L. N. Chen, L. J. Jiang, and W. E. I. Sha, "Detection of orbital angular momentum with metasurface at microwave band," *IEEE Antennas Wireless Propag. Lett.*, vol. 17, no. 1, pp. 110–113, Jan. 2018.
[8] M. L. N. Chen, L. J. Jiang, and W. E. I. Sha, "Orbital angular momentum generation and detection by geometric-phase based metasurfaces," *Appl. Sci.*, vol. 8, no. 3, p. 362, 2018.
[9] K. Zhang, Y. Yuan, D. Zhang, X. Ding, B. Ratni, S. N. Burokur, M. Lu, K. Tang, and Q. Wu, "Phase-engineered metalenses to generate converging and non-diffractive vortex beam carrying orbital angular momentum in microwave region," *Opt. Express*, vol. 26, no. 2, pp. 1351–1360, Jan. 2018.
[10] J. Wang, J.-Y. Yang, I. M. Fazal, N. Ahmed, Y. Yan, H. Huang, Y. Ren, Y. Yue, S. Dolinar, M. Tur, and A. E. Willner, "Terabit free-space data transmission employing orbital angular momentum multiplexing," *Nature Photon.*, vol. 6, pp. 488–496, Jun. 2012.
[11] M. L. N. Chen, L. J. Jiang, and W. E. I. Sha, "Artificial perfect electric conductor-perfect magnetic conductor anisotropic metasurface for generating orbital angular momentum of microwave with nearly perfect conversion efficiency," *J. Appl. Phys.*, vol. 119, no. 6, 2016, Art. no. 064506.
[12] Z. Chang, B. You, L. S. Wu, M. Tang, Y. P. Zhang, and J. F. Mao, "A reconfigurable graphene reflectarray for generation of vortex THz waves," *IEEE Antennas Wireless Propag. Lett.*, vol. 15, pp. 1537–1540, 2016.
[13] Y. Meng, J. Yi, S. N. Burokur, L. Kang, H. Zhang, and D. H. Werner, "Phase-modulation based transmitarray convergence lens for vortex wave carrying orbital angular momentum," *Opt. Express*, vol. 26, no. 17, pp. 22019–22029, Aug. 2018.
[14] Z. H. Jiang, L. Kang, W. Hong, and D. H. Werner, "Highly efficient broadband multiplexed millimeter-wave vortices from metasurface-enabled transmit-arrays of subwavelength thickness," *Phys. Rev. Appl.*, vol. 9, no. 6, 2018, Art. no. 064009.
[15] F. Tamburini, E. Mari, B. Thidé, C. Barbieri, and F. Romanato, "Experimental verification of photon angular momentum and vorticity with radio techniques," *Appl. Phys. Lett.*, vol. 99, no. 20, 2011, Art. no. 204102.
[16] C. Deng, W. Chen, Z. Zhang, Y. Li, and Z. Feng, "Generation of OAM radio waves using circular vivaldi antenna array," *Int. J. Antennas Propag.*, vol. 2013, Apr. 2013, Art. no. 847859.
[17] Y. Chen, S. Zheng, Y. Li, X. Hui, X. Jin, H. Chi, and X. Zhang, "A flat-lensed spiral phase plate based on phase-shifting surface for generation of millimeter-wave OAM beam," *IEEE Antennas Wireless Propag. Lett.*, vol. 15, pp. 1156–1158, 2016.
[18] K.-Y. Liu, W.-L. Guo, G.-M. Wang, H.-P. Li, and G. Liu, "A novel broadband Bi-functional metasurface for vortex generation and simultaneous RCS reduction," *IEEE Access*, vol. 6, pp. 63999–64007, 2018.
[19] E. Karimi, S. A. Schulz, I. De Leon, H. Qassim, J. Upham, and R. W. Boyd, "Generating optical orbital angular momentum at visible wavelengths using a plasmonic metasurface," *Light, Sci. Appl.*, vol. 3, no. 5, p. e167, 2014.
[20] X. Ma, M. Pu, X. Li, C. Huang, Y. Wang, W. Pan, B. Zhao, J. Cui, C. Wang, Z. Zhao, and X. Luo, "A planar chiral meta-surface for optical vortex generation and focusing," *Sci. Rep.*, vol. 5, no. 1, 2015, Art. no. 10365.
[21] C. Ji, J. Song, C. Huang, X. Wu, and X. Luo, "Dual-band vortex beam generation with different OAM modes using single-layer metasurface," *Opt. Express*, vol. 27, no. 1, pp. 34–44, Jan. 2019.
[22] S. M. Mohammadi, L. K. S. Daldorff, J. E. S. Bergman, R. L. Karlsson, B. Thide, K. Forozesh, T. D. Carozzi, and B. Isham, "Orbital angular momentum in radio—A system study," *IEEE Trans. Antennas Propag.*, vol. 58, no. 2, pp. 565–572, Dec. 2010.
[23] M. Lin, Y. Gao, P. Liu, and J. Liu, "Theoretical analyses and design of circular array to generate orbital angular momentum," *IEEE Trans. Antennas Propag.*, vol. 65, no. 7, pp. 3510–3519, Jul. 2017.
[24] H.-X. Xu, L. Zhang, Y. Kim, G.-M. Wang, X.-K. Zhang, Y. Sun, X. Ling, H. Liu, Z. Chen, and C.-W. Qiu, "Wavenumber-splitting metasurfaces achieve multichannel diffusive invisibility," *Adv. Opt. Mater.*, vol. 6, no. 10, 2018, Art. no. 1800010.
[25] H. Li, G. Wang, T. Cai, H. Hou, and W. Guo, "Wideband transparent beam-forming metadevice with amplitude- and phase-controlled metasurface," *Phys. Rev. Appl.*, vol. 11, no. 1, 2019, Art. no. 014043.
[26] K. Chen, Y. Feng, F. Monticone, J. Zhao, B. Zhu, T. Jiang, L. Zhang, Y. Kim, X. Ding, S. Zhang, A. Alù, and C.-W. Qiu, "A reconfigurable active huygens' metalens," *Adv. Mater.*, vol. 29, no. 17, May 2017, Art. no. 1606422.
[27] H.-X. Xu, G. Hu, L. Han, M. Jiang, Y. Huang, Y. Li, X. Yang, X. Ling, L. Chen, J. Zhao, and C.-W. Qiu, "Chirality-assisted high-effciency metasurfaces with independent control of phase, amplitude, and polarization," *Adv. Opt. Mater.*, vol. 7, no. 4, Feb. 2019, Art. no. 1801479.
[28] N. Yu, P. Genevet, M. A. Kats, F. Aieta, J.-P. Tetienne, F. Capasso, and Z. Gaburro, "Light propagation with phase discontinuities: Generalized laws of reflection and refraction," *Science*, vol. 334, no. 6054, pp. 333–337, Oct. 2011.
[29] G. Ding, K. Chen, T. Jiang, B. Sima, J. Zhao, and Y. Feng, "Full control of conical beam carrying orbital angular momentum by reflective metasurface," *Opt. Express*, vol. 26, no. 16, pp. 20990–21002, 2018.
[30] H.-X. Xu, H. Liu, X. Ling, Y. Sun, and F. Yuan, "Broadband vortex beam generation using multimode Pancharatnam–Berry metasurface," *IEEE Trans. Antennas Propag.*, vol. 65, no. 12, pp. 7378–7382, Dec. 2017.
[31] S. Tang, T. Cai, J.-G. Liang, Y. Xiao, C.-W. Zhang, Q. Zhang, Z. Hu, and T. Jiang, "High-efficiency transparent vortex beam generator based on ultrathin Pancharatnam–Berry metasurfaces," *Opt. Express*, vol. 27, no. 3, pp. 1816–1824, 2019.
[32] L. Guan, Z. He, D. Ding, Y. Yu, W. Zhang, and R. Chen, "Polarization-controlled shared-aperture metasurface for generating a vortex beam with different modes," *IEEE Trans. Antennas Propag.*, vol. 66, no. 12, pp. 7455–7459, Dec. 2018.
[33] R. C. Devlin, A. Ambrosio, N. A. Rubin, J. P. B. Mueller, and F. Capasso, "Arbitrary spin-to–orbital angular momentum conversion of light," *Science*, vol. 358, no. 6365, pp. 896–901, Nov. 2017.

WEN-LONG GUO was born in China, in 1993. He received the B.S. degree in radar engineering and the M.S. degree in electromagnetic field and microwave technology from Air Force Engineering University, Xi'an, China, in 2014 and 2016, respectively, where he is currently pursuing the Ph.D. degree. He has published over ten peer-reviewed first-author articles in *Physical Review Applied*, *Optics Express*, the IEEE Antennas and Wireless Propagation Letters, and the *Journal of Physics D: Applied Physics*. His current research interests include metamaterials and their applications to performance enhancement of novel antennas.

GUANG-MING WANG was born in China, in 1964. He received the B.S. and M.S. degrees from Air Force Engineering University, Xi'an, China, in 1982 and 1990, respectively, and the Ph.D. degree from the University of Electronic Science and Technology, Chengdu, China, in 1994, all in electromagnetic field and microwave technology. He joined Air Force Engineering University as an Associate Professor, where he was promoted to a Full Professor, in 2000, and is currently the Head of the Microwave Laboratory. He has authored or coauthored more than 100 conference and journal articles. His current interests include microwave circuits, antennas, and also the new structures, including EBG, PBG, metamaterials, and fractals. He has been a Senior Member of the Chinese Commission of Communication and Electronics. Since 1994, he has been awarded and warranted several items supported under the National Natural Science Foundation of China and fulfilled many local scientific research programs.

HAI-PENG LI was born in China, in 1991. He received the B.S. and M.S. degrees in electromagnetic field and microwave technology from Air Force Engineering University, Xi'an, China, in 2013 and 2015, respectively, where he is currently pursuing the Ph.D. degree. His research interests include metamaterials, metasurfaces, and their applications to novel antennas and multifunctional devices.

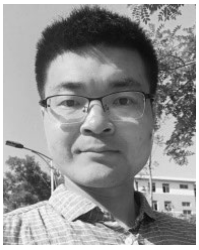

HAI-SHENG HOU was born in China, in 1991. He received the B.S. degree in electronic and information engineering from the Hebei University of Technology, Tianjin, China, in 2014, and the M.S. degree in electromagnetic field and microwave technology from Air Force Engineering University, Xi'an, China, in 2015, where he is currently pursuing the Ph.D. degree.

His current research interests include active metasurfaces, functional materials, and their application for the performance enhancement of novel antenna.

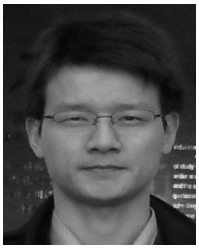

HE-XIU XU (S'11–M'14–SM'17) was born in China, in 1985. He received the B.S. degree in radar engineering and the Ph.D. degree in electronic science and technology from Air Force Engineering University, Xi'an, China, in June 2008 and June 2014, respectively.

He was a Visiting Scholar with the State Key Laboratory of Millimeter Waves, Southeast University, Nanjing, China, from February 2012 to January 2014, a Postdoctoral Fellow with the State Key Laboratory of Surface Physics, Fudan University, Shanghai, China, from 2015 to 2017, and also a Visiting Scholar with the Department of Electrical and Computer Engineering, National University of Singapore, from December 2017 to December 2018. He joined Air Force Engineering University, in September 2014, and was promoted to an Associate Professor, in September 2016. He is currently a Guest Professor with Hengyang Normal University. He has published more than 80 peer-reviewed first-author and coauthor journal articles in *Nature Materials*, *Nature Photonics*, *Light: Science & Applications*, the PROCEEDINGS OF IEEE, *ACS Photonics*, *Advanced Optical materials*, *Photonics Research*, the IEEE TRANSACTIONS ON ANTENNAS AND PROPAGATIONS, *Physical Review Applied*, *Physical Review B*, *Annalen der Physik*, *Applied Physics Letters*, *Optics Express*, *Scientific Reports*, the IEEE MICROWAVE AND WIRELESS COMPONENTS LETTERS, the IEEE TRANSACTIONS ON MAGNETICS, and the *IEEE Microwave Magazine*. He has also published two Chinese books and two English book chapters. He has owned 24 Chinese patents and has given more than 14 invited talks. His research interests include passive/active metamaterials/metasurfaces, and their applications to novel microwave functional devices and antennas.

Dr. Xu is currently a Fellow of IET and a Senior Member of CIE. He received the 8th China Youth Science and Technology Innovation Award, in 2013. He received the Best Excellent Doctoral Dissertation Award at Air Force Engineering University, in 2014, and later received the Excellent Doctoral Dissertation Award from Military, Shaanxi Province, and Chinese Institute of Electronics (CIE). He has hosted several programs, such as the National Science Foundation of China, the Key Program of National Natural Science Foundation of Shaanxi Province, the Natural Science Foundation of Shaanxi Province, the China Scholarship Fund, and the First-Class General and Special Financial Grant from the China Postdoctoral Science Foundation. He receives the URSI AP-RASC Young Scientist Award and the URSI EMTS Young Scientist Award, in 2019, and several Scientific and Technological Progress Awards to date. He was awarded an Outstanding Scientific and Technological Worker of CIE, in 2018, a Young Talent from the China Association for Science and Technology, in 2017, and the Young Scientist Nova from the Shaanxi Technology Committee, in 2016. He was also a recipient of the Excellent Paper Award in metasurface multifunctional devices at the 23rd Annual Youth Conference of CIE, in 2017, and in helicity control of metasurface at the PIER Symposium, in 2018, and a co-recipient of the Best Paper Award in bifunctional metasurfaces at the A3 Metamaterials Forum, in 2017. He served as the Special Session Chair eight times and a TPC Co-Chair/member more than 12 times for international conferences. He has been serving as an Editor for the *AEU International Journal of Electronics and Communications*, since 2014, and has served as a Guest Editor for the Special Issue Metamaterial Circuits and Antennas of the *International Journal of RF and Microwave Computer-Aided Engineering*, in 2018, and as an invited Reviewer for more than 20 leading journals, including *Light: Science & Applications*, *ACS Applied Materials & Interfaces*, the IEEE TRANSACTIONS ON MTT/AP, *Scientific Reports*, *Applied Physics Letters*, IEEE ACCESS, the IEEE MICROWAVE AND WIRELESS COMPONENTS LETTERS, *Radio Science*, *Progress in Electromagnetic Research*, *Optical Material Express*, *IET Microwaves, Antennas & Propagation*, and the *Journal of Electromagnetic Waves and Applications*.